Coherent electric structures: Vlasov-Ampère simulations and observational consequences

Carine Briand, André Mangeney, Francesco Califano

Coherent electric structures: Vlasov-Ampère simulations and observational consequences

C. Briand,[1] A. Mangeney,[1] and F. Califano[2]

Received 17 December 2007; revised 5 March 2008; accepted 15 April 2008; published 30 July 2008.

[1] Coherent electrostatic structures, like bipolar electric pulses (also called electrostatic solitary waves) or Langmuir waves, are frequently observed in many astrophysical plasma of the Earth environment (plasma sheet boundary layer, Earth bow shock, auroral regions etc.) or in the solar wind. They are thought to play a crucial role in the energy transfer from small to large scale and to reconnection processes. Numerous simulations have studied their emergence and evolution. Most of them are based on the development of two stream instabilities. Another mechanism is investigated here: the plasma is excited by a localized, time dependent modulation of the electron distribution function (heating of the electrons). The investigation is performed through a 1D Vlasov-Ampere code, in open boundary conditions. We explore the response of the plasma to several heating conditions, mass ratio and density gradient. We find that the heating leads to the development of an extended turbulent domain. We also show that the history of the electrostatic solitary waves (ESW) strongly depends on the presence of a density gradient and the mass ratio between species. If the positive charged neutralizing background is composed of heavy ions, the ESW turns back to the entrance domain when a density gradient is included. From the observational point of view, this means that the electric field shows a polarity reversal with time.

Citation: Briand, C., A. Mangeney, and F. Califano (2008), Coherent electric structures: Vlasov-Ampère simulations and observational consequences, *J. Geophys. Res.*, *113*, A07219, doi:10.1029/2007JA012992.

1. Introduction

[2] Space plasmas at kinetic length scales, let say the Debye length, are characterized by the presence of coherent structures superposed over a ''sea'' of high and low frequency oscillations often supported by a non-Maxwellian plasma, as for example observed in the solar wind. In this case, the non-Maxwellian character of the distribution function is, first of all, a signature of the weakness of collisional effects, but also of the continuous injection of energy resulting from a MHD wave cascade and of the presence of incoming supra thermal particles accelerated by complicated mechanisms, as for example reconnection in the solar corona or magnetosphere.

[3] High frequency Langmuir oscillations at nearly the plasma frequency f_p are often observed in the form of wave packets in the interplanetary space where also the harmonic at 2 f_p is detected. Typical values of the electric field associated to such wave packets are in the range $01 \leq E \leq 10$mV/m over typical length scales from 50 λ_D and 1000 λ_D corresponding to the so-called weak and intense wave packets. There is not an accepted model capable of explaining the mechanism underlying the generation of burtsy plasma wave packets [see *Nulsen et al.*, 2007, and references therein] although numerous suggestions have been made. For example, in a recent paper, *Ergun et al.* [2008] have shown that isolated Langmuir wave packets can be decomposed in low order eigenmodes of solitons formed in parabolic density depression in the solar wind.

[4] Coherent solitary structures are observed in space plasmas in the form of bipolar electric pulses mainly parallel to the ambient magnetic field. They have been first observed in strongly nonhomogeneous regions of the Earth's environment as for example the bow Shock [*Bale et al.*, 1998], the plasma sheet boundary [*Matsumoto et al.*, 1994], the auroral zone [*Temerin et al.*, 1982; *Ergun et al.*, 1998b] and have been then also detected in the solar wind [*Mangeney et al.*, 1999]. Today, they are routinely detected owing to spacecraft observations in all planetary environments. The electric field associated to such coherent structures spans over a wide range of value depending on the observed location: of the order or less than 0.1 mV/m in the solar wind and the plasma sheet boundary layer, it can reach 100 mV/m or more in the bow shock and the auroral regions.

[5] The standard theoretical argument used to explain the observed plasma oscillations as well as the coherent structures, relies on the development of two streams or bump-on-tail like instabilities which excite Langmuir waves. These waves then interact with plasma inhomogeneities or evolve nonlinearly giving rise to different phenomena, as for example Langmuir wave collapse, generation of ion acous-

[1]LESIA, Observatoire de Paris, CNRS, UPMC, Université Paris Diderot, Meudon, France.
[2]Dipartimento Fisica and CNISM, Università di Pisa, Pisa, Italy.

0148-0227/08/2007JA012992

Table 1. List of Some Typical Physical Values in the Quiet Solar Wind and Auroral Zone[a]

	n_e cm^{-3}	T_e 10^5 K	w_p kHz	λ_d m	E mV/m
S.W.	5	1.5	3	10	up to a few tens
Aurora	5	2–80	3	14–90	up to a few hundreds

[a]Electrical field values correspond to typical Langmuir waves.

tic modes, etc. [see, e.g., *Li et al.*, 2003, and references therein].

[6] However, even if all these studies were able to reproduce some of the observed features it appears to be quite difficult, in typical astrophysical conditions, to directly generate nearly monoenergetic beams except maybe in very peculiar cases. The maximum velocity of the observed beam shifts toward lower velocity values [*Lin et al.*, 1981] indicating that a broad range of velocities is involved in the interaction as time goes on, while the usual theoretical approach is based on a monoenergetic beam approach. In order to free the theoretical models from the necessity of initial monoenergetic beams, another mechanism for the generation of coherent electrostatic structures have been proposed by *Briand et al.* [2007]. The authors considered a plasma, initially at rest, perturbed from one boundary by localized, time dependent variations of the electron distribution function which corresponds to some local heating. The main result of this investigation was to show the possibility of generating electrostatic coherent structures of BGK type. In this former paper, the perturbation of the electron distribution function was continuous and the plasma was uniform. However, observations show that space plasmas are characterized by density gradients extending over a large range of scale heights (from thousands of Debye lengths in the solar wind to a few tens of Debye lengths in the Earth environment). The consequences of density gradient on the behavior of the electrostatic structure has also been recognized through PIC simulations [*Mandrake et al.*, 2000]. The present study thus extends our former investigation to the case of impulsive heating in a density stratified medium. The results also give some clue for observational tests in several environments.

2. Simulation Model

[7] The atmospheric model includes both electrons and protons and is limited to a 1D geometry since many observations show that most of the electric structures are field aligned [see e.g., *Ergun et al.*, 1998a]. It is density stratified following the Pannekoek-Rosseland [*Rosseland*, 1924] kinetic approach: the gravity $g^\star$ is balanced by a time independent electric field and dollar; and dollar; to maintain the charge neutrality. The two fields depend only on the species mass and temperature ratios and on the scale height h which are free parameters of the simulation. In absence of external forcing, the electric force compensates for the gravitational force and the atmosphere is in a state of stable equilibrium. Moreover, it can be shown that when $T_p/T_e = 1$ and $m_p \gg m_e$ and dollar; (which is the case of all the simulations presented here), the ambipolar electric field takes the simple relation $\varepsilon = 1/h$ and the gravity field can be expressed in terms of the ambipolar field and species mass ratio only ($g^\star = 2\, m_e/m_p$).

[8] The evolution of the distribution function of the particles is described by the Vlasov-Ampère system of equations, in a 1D geometry and with open boundary conditions. They are numerically solved following the scheme described by *Mangeney et al.* [2002]. The algorithm is based on the "splitting algorithm" which in practice reduces the numerical scheme to the solution of an advection equation obtained by the implementation of a third order accurate Van Leer scheme which conserves the total charge of the particles.

[9] The evolution of the self induced electric field E is determined through the Ampere's law. The Vlasov-Ampere system of equations, in dimensionless units, reads:

$$\frac{\partial f_\alpha}{\partial t} + v_\alpha \frac{\partial f_\alpha}{\partial x} + [\sigma_\alpha (E + \varepsilon) - g^\star] \frac{\partial f_\alpha}{\partial v_\alpha} = 0, \tag{1}$$

$$\frac{\partial E}{\partial t} = -J. \tag{2}$$

$$\int v_p f_p \, dv_p - \int v_e f_e \, dv_e = J. \tag{3}$$

where f is the distribution function, E the electric field, J the current density and the index α indicates the species (e for electrons and p for protons). In these equations we have taken the electron mass m_e, the electron thermal velocity v_{te}, the plasma frequency ω_e (taken at $x = 0$ and dollar;) as a characteristic mass, velocity and frequency. Then, the characteristic length, electric field and gravity, at $x = 0$ and $\lambda_D = v_{te}/\omega_e$ (Debye length), $\bar{E} = m_e v_{te} \omega_e / e$ and $\bar{g} = v_{te}\omega_e$. Finally, in our dimensionless unit $\sigma_e = -1$ and $\sigma_p = m_e/m_p$. Typical characteristic values for most of these parameters in different natural plasma contexts are summarized in Table 1.

[10] The distribution function of each species at time t = 0 is described by a normalized Maxwellian function:

$$f_e(x \neq 0, v_e, 0) = \exp\left(-\frac{x}{h}\right) \exp\left(-\frac{v_e^2}{2}\right), \tag{4}$$

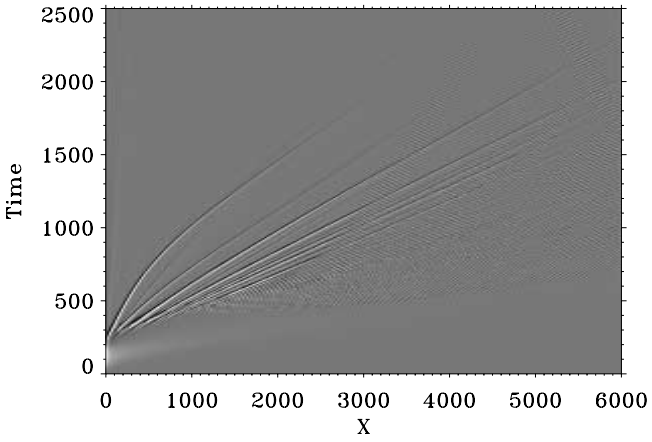

Figure 1. Typical example of electric field amplitude versus space and time in the case of homogeneous plasma.

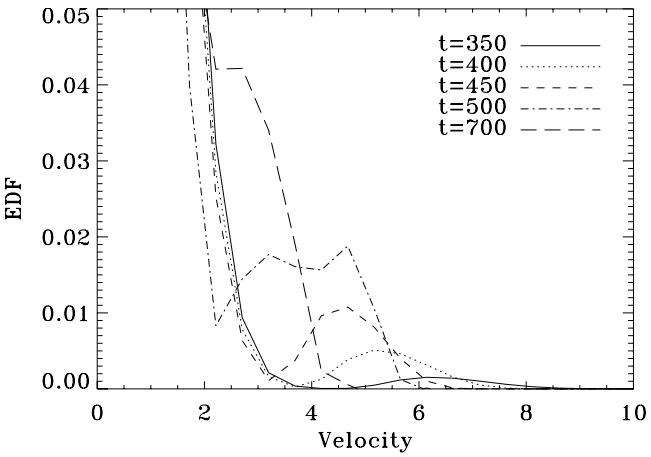

Figure 2. Electron Distribution Function versus velocity at position x = 1500 for several time (indicated on the graph).

$$f_p(x, v_p, 0) = \exp\left(-\frac{x}{h}\right)\exp\left(-\frac{v_p^2}{2}\frac{m_p}{m_e}\frac{T_e}{T_p}\right), \quad (5)$$

[11] Initially, the system is isothermal with the same temperature for both particle species (T_p/T_e = 1).

[12] In x = L (i.e., on the right side of the box), the particles with $v > 0$ are free to leave while those entering in the box ($v < 0$) are imposed by the following time independent boundary condition:

$$f_\alpha(x = L, v_\alpha < 0, t) = f_\alpha(x = L, v_\alpha, t = 0), \quad (6)$$

[13] For $t \geq 0$ the system is perturbed by the injection of heated electrons in x = 0 (left side). It is achieved by a time

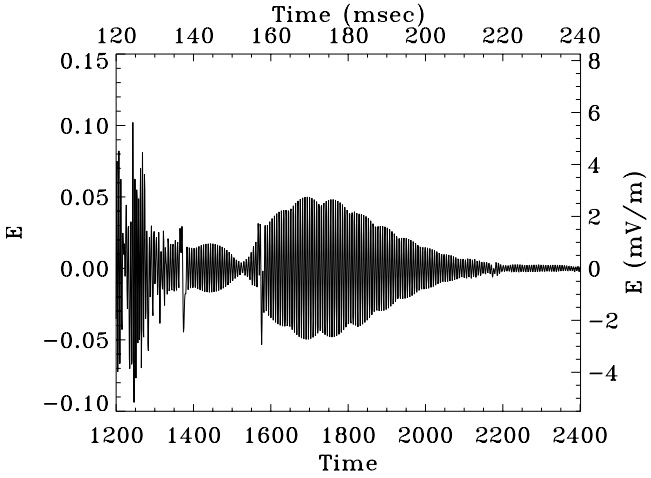

Figure 3. Electric field amplitude as a function of time for the position x = 2250 of Figure 1. The axis are expressed either in the dimensionless units of the code (left and bottom) or physical units (right and top).

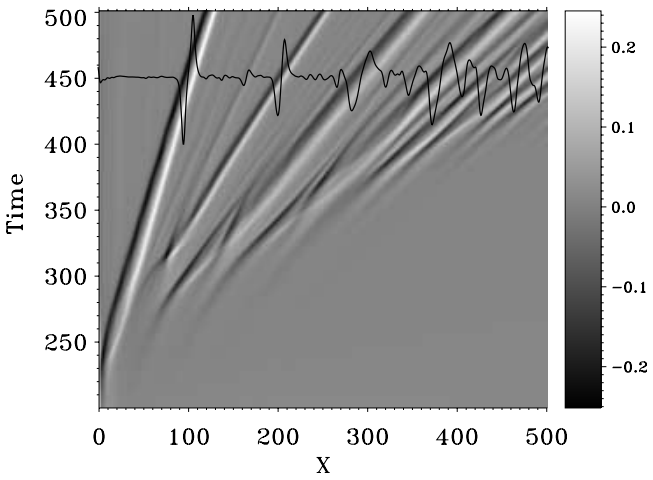

Figure 4. Electric field amplitude versus space and time together with the electric field profile at time t =450. Note its similarity with the observed profiles reported by *Matsumoto et al.* [1994].

dependent modulation of the electron Maxwellian distribution function:

$$f_e(x = 0, v_e, t) = \exp\left(-\frac{v_e^2}{2v_{\text{driver}}^2}\right), \quad (7)$$

$$v_{\text{driver}} = 1 + \alpha(t)\left[1 - \cos\left(\frac{2\pi t}{P}\right)\right]. \quad (8)$$

[14] The amplitude of the heating is thus set by and v_{driver} (equation (8)) which depends on time through the function and dollar; and dollar; and with a characteristic time equal to the period P. It is worth noting that this forcing mechanism conserves the charge density, thus charge neutrality.

[15] In the present work, L = 4000 λ_D, T_p/T_e = 1 P = 300, dt = 4.10^{-3} dx = 0.5 λ_D, dv_e = 0.15 and dv_p = 0.015. In the figures presented below, the parameters are expressed in normalized units, except when physical units are considered (in which case, they are made explicit).

3. Simulation

3.1. Wave Generation: General Overview

[16] In this section, the perturbation of the electron distribution function consists in a pulse of short duration. The parameter α of equation (8) follows the rule:

$$\alpha(t) \neq 0 \; for \; t \leq t_{\max} \quad (9)$$

$$\alpha(t) = 0 \; for \; t > t_{\max} \quad (10)$$

with $t_{\max}$ =300. For all runs of this part, $h = \infty$ (no density gradient), $\mu = m_p/m_e$ =1836. The consequences of the modification of these parameters on the plasma behavior are discussed in the next subsection. Several simulations were performed with $0.5 \leq \alpha \leq 2.5$. In the following examples,

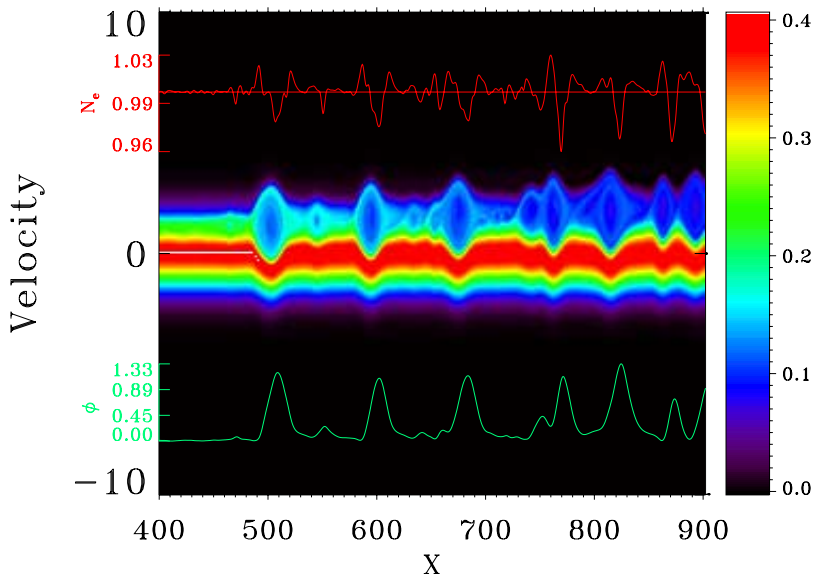

Figure 5. Electron distribution function as a function of space and velocity at time $t = 650$. Top graph (in red): Electron density; Bottom graph (in green): electric potential.

$\alpha = 0.75$, which means a variation of 2.5 of the thermal velocity of the electrons. We must stress that another kind of forcing consisting in a series of pulses (similar to a sawtooth form) have also been tested. We have chosen not to detailed these simulations since they introduce another free parameter (the time between two successive pulses) and the results are qualitatively similar to those presented here.

[17] All runs lead to the development of several kinds of coherent waves, namely Langmuir and Electrostatic Solitary Waves (hereafter ESW [*Matsumoto et al.*, 1994]). They finally form a spatially and temporally extended turbulent domain. Figure 1 shows a typical example of the electric field as a function of space and time. ESW are clearly distinguished as large amplitude isolated structures while the turbulent domain appears below the limit formed by these ESW.

[18] Langmuir waves develop through a bump-on-tail instability. Indeed, most of the injected electrons freely travel across the simulation box following a ballistic trajectory leading to the generation of a bump on the tail of the electron distribution function. Coherent Langmuir waves grow and trap the resonant electrons, diffusing the bump to a flat distribution (Figure 2) which stops the wave growth. The graph also shows that, for a determined spatial position, the bump slowly moves toward lower velocities as time goes on. This shift of the central beam velocity results from the ballistic trajectory of the particles. Such behavior of the electron distribution function has also been observed in the solar wind [*Lin et al.*, 1981]. As a consequence, Langmuir waves with different phase velocity are excited, leading to a broad range of wave numbers and frequencies. It is worth noting that this broad spectrum naturally appears as a

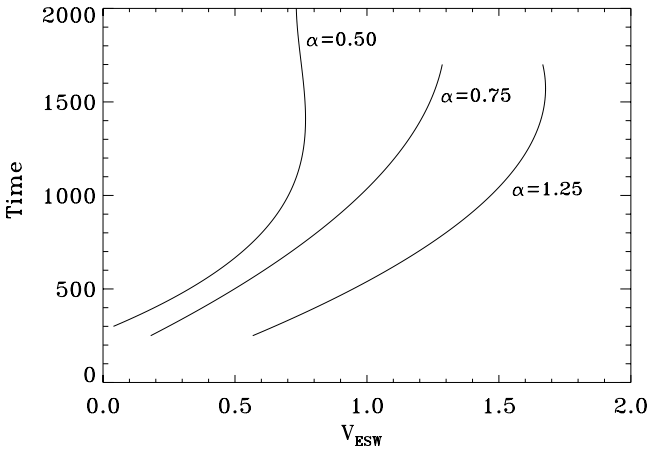

Figure 6. Velocity of one selected ESW as a function of time for three runs with different heating values (indicated on the plot through the α parameter): larger values of α indicate larger heating.

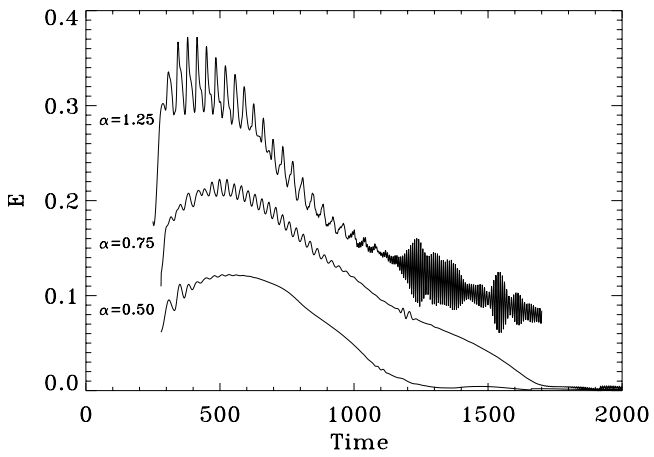

Figure 7. Electric field maximum amplitude along a selected ESW as a function of time for three runs with different heating values (indicated on the plot through the α parameter).

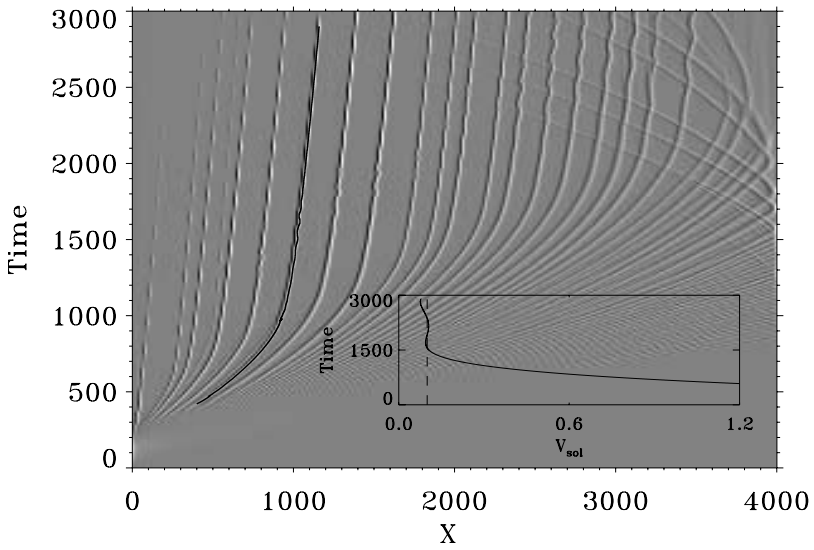

Figure 8. Electric field as a function of space and time (Run7). The inset shows the plot of the velocity as a function of time for the solitary structure underlined in black.

consequence of the time dependent injection of heated particles. The theories based on monoenergetic beams require nonlinear interactions and/or coupling with the inhomogeneous background medium in order to enlarge the wave vector spectrum of the excited waves, otherwise confined to a too narrow k interval (corresponding to the waves excited by the beam).

[19] The Langmuir waves generated in the simulation appear in the form of wave packets of limited sizes (Figure 3), as frequently observed in the solar wind. The analogy is not only qualitative, but also the amplitudes (using the parameters of Table 1) are comparable. To compare with observations, the time range of Figure 3 has been limited to a subset corresponding to records from the TDS/WAVES instrument [*Bougeret et al.*, 2008] on board of STEREO (examples are also given by *Ergun et al.* [2008]).

[20] Isolated Electrostatic Solitary Waves are one of the main feature observed in the simulations. These isolated waves form at the beginning of the simulations (Figure 4) as a consequence of the applied boundary conditions. Indeed, the applied heating preserves the total electron density but increases the density of high velocity particles. The plasma reacts to this current injection by generating a return current which shifts the core of the distribution function toward negative velocities. This implies a local charge separation that therefore generates an electric field. Low velocity electrons (i.e., $|v| < \sqrt{2\phi}$ in the particles frame) are trapped in the positive electric potential leading to the development of vortices in the phase space (Figure 5). The other ESW that develop well inside the simulation box result from a different mechanism, namely, the bump-on-tail instability. Because of the positive potential which repeals electrons, the vortices are associated with electron density cavities.

[21] These isolated bipolar electric fields cross the simulation box at a constant velocity spanning between 0.05 and $2v_{te}$. This velocity range depends on the applied heating: the stronger the heating, the larger the velocity (Figure 6). The electric structures are rapidly damped, and thus do not travel for long distances (Figure 7). However, the lifetime of an isolated structure is increased when a density gradient is present in the box (see below section 3.2).

[22] To understand the role of the dynamics of the positive charges, we have made simulations with a larger mass ratio: protons are replaced by oxygen ions (μ = 29,376). Qualitatively, the behavior of the plasma is similar to the previous section. So, for an initial *homogeneous* plasma, the protons or ions do not play a crucial role in the behavior of the plasma (at least, as long as real mass ratio are used, see *Califano et al.* [2007] for more comments when unrealistic mass ration are employed).

3.2. Density Gradient

[23] We now explore the consequences of the presence of a density gradient through the simulation box (see equations (4) and (5)). Similarly to the simulations of the previous section, several heating conditions were applied (through a variation of the α parameter). We present here results for α = 0.75.

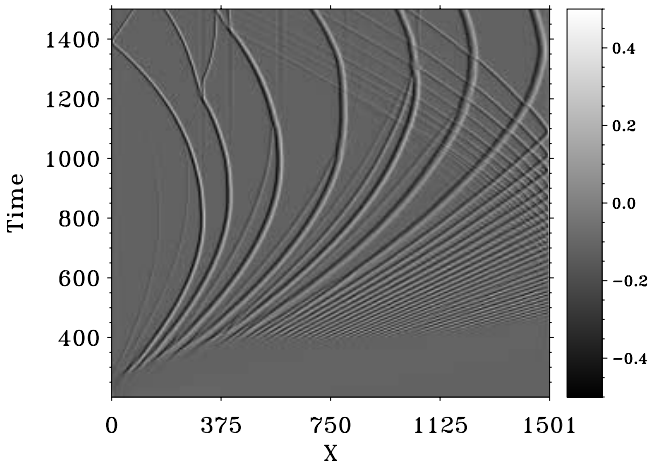

Figure 9. Electric field as a function of space and time (Run8).

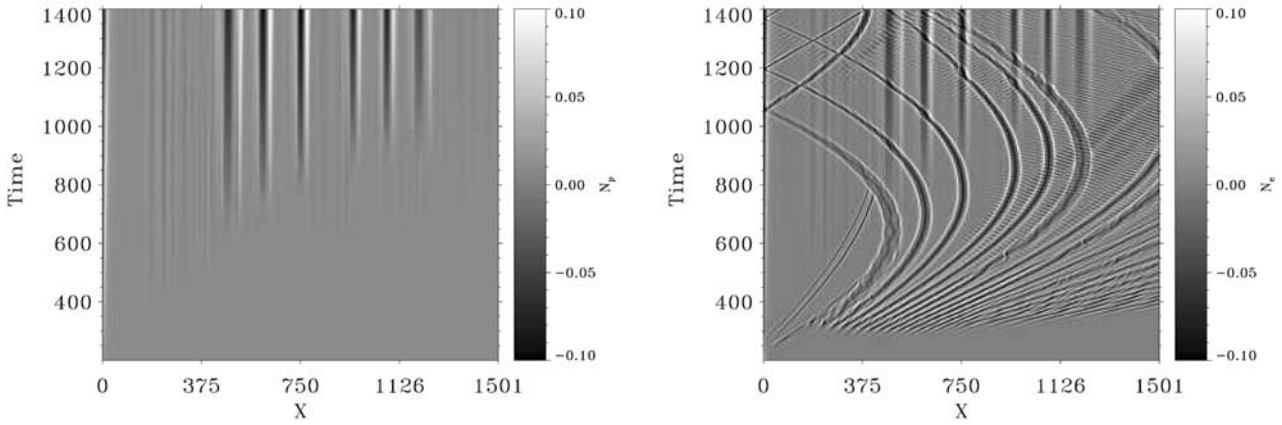

Figure 10. (left) Ion density and (right) electron density as a function of space and time (Run8). For sake of clarity, the density gradient has been removed.

[24] Two simulations are presented here to illustrate the behavior of the plasma. In both simulations, a gradient with a scale height $h = 3/4L$ is applied but with different mass ratio: in Run7 $\mu = 1836$ while in Run8 $\mu = 29{,}376$. This choice of scale height is not meant to represent any specific space environment but represents a compromise between real density gradient in different astrophysical contexts and computational resources. However, the simulations correspond to the real case of large scale density variations (homogeneous plasma) and approximate some cases of small scale inhomogeneities.

[25] Numerous ESW appear, now clearly isolated (Figures 8 and 9). Figure 8, shows the decrease of the ESW velocity from $1.2V_{te}$ when the structure is formed to a constant value of $0.1V_{te}$ around $t = 1000$. Note that this latest value is still much higher than the ion sound speed $v_i = \sqrt{\mu}\ 0.02v_{te}$. Conversely to the previous section, the lifetime of the ESW is increased: the waves survive the all duration of the simulation but they travel across limited distances (a few hundreds Debye length). In order to check spurious numerical effects driven by the presence of the right boundary, we have performed a number of simulations with different box size. The results were equivalent. This choice of box size was the best compromise to clearly distinguish the turbulent domain and the solitary structures.

[26] Run8 is the same as Run7 but with protons replaced by oxygen ions. This choice correspond to auroral regions where O^+ are the dominant ion species. Figure 9 shows the electric field resulting of Run8. Clear isolated ESW appear. After a more or less extended displacement in the box, each potential structure turns back toward the left boundary $x = 0$. Many other phenomena are also observed (like splitting of the vortex, waves trapping in the EWS etc): they will be detailed in a subsequent paper. As illustrated on Figure 10 at the direction reversal, a ion density cavity forms and decouples from the electrostatic structure. A decrease of electron density immediately develops to locally maintain the charge neutrality. These stationary density cavities are observable quantities: at the end of the simulation they reach about 10% of the initial density level. This decoupling from density cavities and electrostatic field was also observed by *Eliasson and Shukla* [2005, Figure 2, Figure 3] where, however, the density perturbation is applied on an already formed electron hole. The change of direction of the ESW has an interesting consequence from the observational point of view. Figure 11 displays an electric field profile for a given position, as would observe a space instrument. Because of the direction reversal of the electric structure, the ESW is detected twice but with opposite field polarity. *Omura et al.* [1999] show opposite polarity of the observed electric field and interpret it as a change of the flow direction of the electric potential. We show here that such phenomena can also be explained without invoking strong modification of the velocity flows: a reversal of the structure displacement due to the presence of a gradient in a heavy ion background can also be at the origin of such polarity inversion.

4. Conclusions

[27] A former paper *Briand et al.* [2007] presented the response of a plasma to a continuous periodic time modu-

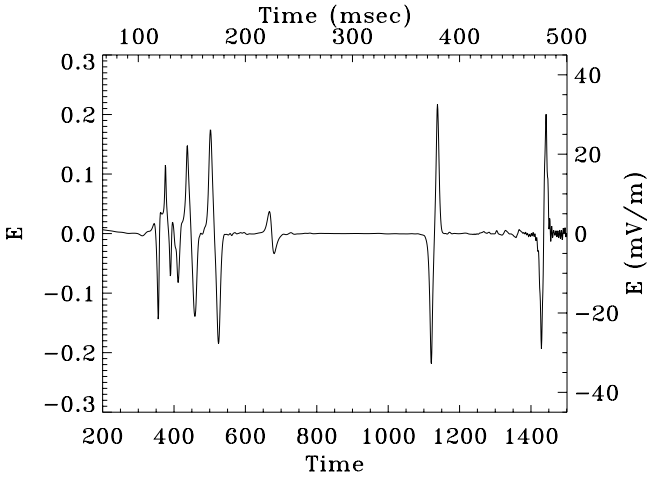

Figure 11. Electric field as a function of time for the spatial position $x = 200$ and dollar; (Run8 - see also Figure 9). The physical units are obtained taking a plasma frequency of 3 kHz given by *Omura et al.* [1999].

lation of the electron distribution function at the boundary of the simulation box (i.e., spatially localized). The present paper explores the response of a plasma to a different modulation mechanism (single pulse) varying the heating amplitude and discusses the role of mass ratio and density gradient. We first show that, even in absence of an initial extended, monoenergetic beam in the plasma, the applied heating lead to the formation of Langmuir and Electrostatic Solitary Waves. Indeed, the heated electrons travel through the simulation box following a ballistic trajectory. As they propagate, they generate bump-on-tail instabilities, at the origin of the waves. Once electrostatic waves are generated, low velocity particles are trapped in the electric potential but the majority of the particles follow their motion, giving rise to the development of the beam like instabilities further in the box. At each spatial position, the hump on the electron distribution function move toward lower velocities as a result of the ballistic effect of the slowest particles. The phase velocity of the resonant particles thus drifts toward smallest values, implying the excitation of a broad range of wave number and the development of a spatially extended turbulent domain.

[28] The presence of a density gradient strongly affects the behavior of the electron holes. First, it helps the stability of the ESW: compare to the situation in an homogeneous plasma, the presence of a density gradient increases their lifetime. However, their lower velocity (about $0.1v_{te}$ compare to about $1v_{te}$ in the homogeneous case) implies that they travel over smaller distances. So, ESW are not expected to be seen far from the generation site. This "local" characteristic may result from the 1D treatment. Indeed, as mentioned by *Oppenheim et al.* [2001], 3D increase the stabilization of the electron holes and allow them to travel over larger distances.

[29] It has been shown in several papers that when the dynamics of the positive particles is taken into account, the mass ratio play a crucial role in the stabilization of the electron holes. We underline here that it also affects their trajectory. In a density stratified atmosphere, ESW show a direction reversal in their displacement in the medium. The electric field presents a polarity reversal if observed at a given position. This is an important point since such observations have already been reported. At each direction reversal, a stationary, protons and electron cavity form. The amplitude of the cavities are strong enough to be observable by space instruments.

[30] **Acknowledgments.** F. Califano thanks the French INSU-CNRS, the Paris Observatory and the Université Pierre et Marie Curie for their financial support. The authors also thank the anonymous referees for their comments that helped to improve the manuscript.

[31] Amitava Bhattacharjee thanks Gregory Howes and S. Gary for their assistance in evaluating this paper.

References

Bale, S. D., P. J. Kellogg, D. E. Larsen, R. P. Lin, K. Goetz, and R. P. Lepping (1998), Bipolar electrostatic structures in the shock transition region: Evidence of electron phase space holes, *Geophys. Res. Lett.*, *25*, 2929–2932.

Bougeret, J. L., et al. (2008), S/WAVES: The radio and plasma wave investigation on the STEREO mission, *Space Sci. Rev.*, *136*(1–4), 487–528, doi:1007/s11214-007-9298-8.

Briand, C., A. Mangeney, and F. Califano (2007), Electrostatic coherent structures generation by local heating in a collisionless plasma, *Phys. Lett. A*, *368*, 82–86, doi:10.1016/j.physleta.2007.03.077.

Califano, F., L. Galeotti, and C. Briand (2007), Electrostatic coherent structures: The role of the ions dynamics, *Phys. Fluids*, *14*, 2306, doi:10.1063/1.2724807.

Eliasson, B., and P. K. Shukla (2005), The dynamics of electron and ion holes in a collisionless plasma, *Nonlinear Process. Geophys.*, *12*, 269–289.

Ergun, R. E., C. W. Carlson, J. P. McFadden, F. S. Mozer, L. Muschietti, I. Roth, and R. J. Strangeway (1998a), Debye-scale plasma structures associated with magnetic-field-aligned electric fields, *Phys. Rev. Lett.*, *81*, 826–829, doi:10.1103/PhysRevLett.81.826.

Ergun, R. E., et al. (1998b), FAST satellite observations of electric field structures in the auroral zone, *Geophys. Res. Lett.*, *25*, 2025–2028.

Ergun, R. E., D. M. Malaspina, S. Eriksson, and D. N. Newman (2008), Eigenmode structure in solar wind Langmuir waves, *Phys. Rev. Lett.*, in press.

Li, B., A. J. Willes, P. A. Robinson, and I. H. Cairns (2003), Dynamics of beam-driven Langmuir and ion-acoustic waves including electrostatic decay, *Phys. Fluids*, *10*, 2748–2762, doi:10.1063/1.1574515.

Lin, R. P., D. W. Potter, D. A. Gurnett, and F. L. Scarf (1981), Energetic electrons and plasma waves associated with a solar type III radio burst, *Astrophys. J.*, *251*, 364–373, doi:10.1086/159471.

Mandrake, L., P. L. Pritchett, and F. V. Coroniti (2000), Electron beam generated solitary structures in a nonuniform plasma system, *Geophys. Res. Lett.*, *27*, 2869–2872.

Mangeney, A., et al. (1999), WIND observations of coherent electrostatic waves in the solar wind, *Ann. Geophys.*, *17*, 307–320.

Mangeney, A., F. Califano, C. Cavazzoni, and P. Travnicek (2002), A numerical scheme for the integration of the Vlasov-Maxwell system of equations, *J. Comput. Phys.*, *179*, 495–538.

Matsumoto, H., H. Kojima, T. Miyatake, Y. Omura, M. Okada, I. Nagano, and M. Tsutsui (1994), Electrotastic Solitary Waves (ESW) in the magnetotail: BEN wave forms observed by GEOTAIL, *Geophys. Res. Lett.*, *21*, 2915–2918.

Nulsen, A. L., I. H. Cairns, and P. A. Robinson (2007), Field distributions and shapes of Langmuir wave packets observed by Ulysses in an interplanetary type III burst source region, *J. Geophys. Res.*, *112*, A05107, doi:10.1029/2006JA011873.

Omura, Y., H. Kojima, N. Miki, T. Mukai, H. Matsumoto, and R. Anderson (1999), Electrostatic solitary waves carried by diffused electron beams observed by the Geotail spacecraft, *J. Geophys. Res.*, *104*, 14,627–14,638, doi:10.1029/1999JA900103.

Oppenheim, M. M., G. Vetoulis, D. L. Newman, and M. V. Goldman (2001), Evolution of electron phase-space holes in 3D, *Geophys. Res. Lett.*, *28*, 1891–1894.

Rosseland, S. (1924), Electrical state of a star, *Mon. Not. R. Astron. Soc.*, *84*, 720–728.

Temerin, M., K. Cerny, W. Lotko, and F. S. Mozer (1982), Observations of double layers and solitary waves in the auroral plasma, *Phys. Rev. Lett.*, *48*, 1175–1179.

C. Briand and A. Mangeney, LESIA, Observatoire de Paris, CNRS, UPMC, Université Paris Diderot, 5 Place Jules Janssen, 92190 Meudon, France. (carine.briand@obspm.fr)

F. Califano, Dipartimento Fisica and CNISM, Università di Pisa, Largo Pontecorvo n.3, 56100 Pisa, Italy.